Ca2+-induced sarcoplasmic reticulum Ca2+ release in myotubularin-deficient muscle fibers

Candice Kutchukian, Peter Szentesi, Bruno Allard, Ana Buj-Bello, Laszlo Csernoch, Vincent Jacquemond

▶ **To cite this version:**

Candice Kutchukian, Peter Szentesi, Bruno Allard, Ana Buj-Bello, Laszlo Csernoch, et al.. Ca2+-induced sarcoplasmic reticulum Ca2+ release in myotubularin-deficient muscle fibers. Cell Calcium, 2019, 80, pp.91-100. ⟨10.1016/j.ceca.2019.04.004⟩. ⟨hal-02325585⟩

HAL Id: hal-02325585

https://hal.science/hal-02325585v1

Submitted on 22 Oct 2021

HAL is a multi-disciplinary open access archive for the deposit and dissemination of scientific research documents, whether they are published or not. The documents may come from teaching and research institutions in France or abroad, or from public or private research centers.

L'archive ouverte pluridisciplinaire **HAL**, est destinée au dépôt et à la diffusion de documents scientifiques de niveau recherche, publiés ou non, émanant des établissements d'enseignement et de recherche français ou étrangers, des laboratoires publics ou privés.

Distributed under a Creative Commons CC BY-NC 4.0 - Attribution - Non-commercial use - International License

Version of Record: https://www.sciencedirect.com/science/article/pii/S0143416019300284
Manuscript_73eb30a5e6d77c9a17e2dec4ff489ac2

Ca^{2+}-induced sarcoplasmic reticulum Ca^{2+} release in myotubularin-deficient muscle fibers

Candice Kutchukian[1], Peter Szentesi[2], Bruno Allard[1], Ana Buj-Bello[3], Laszlo Csernoch[2] and Vincent Jacquemond[1]

[1] Univ Lyon, Université Claude Bernard Lyon 1, CNRS UMR-5310, INSERM U-1217, Institut NeuroMyoGène, 8 avenue Rockefeller, 69373 Lyon, France.

[2] Department of Physiology, Faculty of Medicine, University of Debrecen, Debrecen, Hungary.

[3] INSERM U951, Evry, France; University of Evry, UMR_S951, France

Corresponding authors:

Vincent Jacquemond and Laszlo Csernoch. VJ will handle correspondence at all stages:

Vincent Jacquemond

Institut NeuroMyoGène

UMR CNRS 5310 - INSERM U1217 - Université Claude Bernard Lyon 1

Faculté de Médecine et de Pharmacie

8, Avenue Rockefeller, 69373 Lyon, France

Tel. (33) 4 26 68 82 69

E-mail : vincent.jacquemond@univ-lyon1.fr

List of abbreviations

$Ca_V1.1$, $\alpha 1$ subunit of the dihydropyridine receptor; CNM, centronuclear myopathy; FDB, *flexor digitorum brevis*; EC, excitation-contraction; KO, knock-out; MTM1, myotubularin; RYR1, type 1 ryanodine receptor; SR, sarcoplasmic reticulum; WT, wild-type.

© 2019 published by Elsevier. This manuscript is made available under the CC BY NC user license
https://creativecommons.org/licenses/by-nc/4.0/

Abstract

Skeletal muscle deficiency in the 3-phosphoinositide (PtdIns*P*) phosphatase myotubularin (MTM1) causes myotubular myopathy which is associated with severe depression of voltage-activated sarcoplasmic reticulum Ca^{2+} release through ryanodine receptors. In the present study we aimed at further understanding how Ca^{2+} release is altered in MTM1-deficient muscle fibers, at rest and during activation. While in wild-type muscle fibers, SR Ca^{2+} release exhibits fast stereotyped kinetics of activation and decay throughout the voltage range of activation, Ca^{2+} release in MTM1-deficient muscle fibers exhibits slow and unconventional kinetics at intermediate voltages, suggestive of partial loss of the normal control of ryanodine receptor Ca^{2+} channel activity. In addition, the diseased muscle fibers at rest exhibit spontaneous elementary Ca^{2+} release events at a frequency 30 times greater than that of control fibers. Eighty percent of the events have spatiotemporal properties of archetypal Ca^{2+} sparks while the rest take either the form of lower amplitude, longer duration Ca^{2+} release events or of a combination thereof. The events occur at preferred locations in the fibers, indicating spatially uneven distribution of the parameters determining spontaneous RYR1 opening. Spatially large Ca^{2+} release sources were obviously involved in some of these events, suggesting that opening of ryanodine receptors in one cluster can activate opening of ryanodine receptors in a neighboring one. Overall results demonstrate that opening of Ca^{2+}-activated ryanodine receptors is promoted both at rest and during excitation-contraction coupling in MTM1-deficient muscle fibers. Because access to this activation mode is denied to ryanodine receptors in healthy skeletal muscle, this may play an important role in the associated disease situation.

Keywords

Skeletal muscle, ryanodine receptor, sarcoplasmic reticulum Ca^{2+} release, myotubular myopathy.

1. Introduction

In differentiated skeletal muscle fibers, contraction is triggered by the increase in cytosolic Ca^{2+} concentration resulting from sarcoplasmic reticulum (SR) Ca^{2+} release. For this, the voltage sensing $Ca_V1.1$ subunit of the dihydropyridine receptor in the transverse (t-) invaginations of the plasma membrane interacts with the type 1 ryanodine receptor (RYR1) Ca^{2+} release channel in the proximate membrane of the junctional SR. This interaction constitutes the switch of excitation-contraction (EC) coupling, allowing turning on and off RYR1 channel activity and consequent SR Ca^{2+} release, in response to t-tubule membrane depolarization and repolarization, respectively [1, 2]. RYR channels are also Ca^{2+}-activated channels capable of operating under the Ca^{2+}-induced Ca^{2+} release (CICR) mode, but in healthy differentiated mammalian muscle, the tight control of RYR1 channel activity by $Ca_V1.1$ voltage-sensors is believed to repress Ca^{2+}-mediated activation of the channels [see 3, 4].

EC coupling is defective in myotubular myopathy, a disease due to mutations in the gene encoding the PtdIns*P* phosphatase myotubularin (MTM1) [5]. This was established using the MTM1-deficient mouse model which reproduces the main features of human myotubular myopathy [6]: in the absence of MTM1, muscle fibers suffer from decreased number of triads (the region where one t-tubule faces two terminal cisternae of junctional SR), disrupted t-tubule network and decreased amounts of $Ca_V1.1$ and RYR1 [7]. At the functional level, voltage-activated SR Ca^{2+} release exhibits reduced peak amplitude, delayed activation kinetics and subcellular non-uniformity [7, 8]. Another hallmark of the disease is that loss of MTM1 enzymatic activity is likely playing a critical role in the pathological defects: indeed, MTM1 dephosphorylates PtdIns(3,5)P_2 and PtdIns(3)*P* at the D3 position of the inositol ring [9, 10] and in the disease mouse model both Ca^{2+} release defects in muscle fibers and survival of the animals

are improved by PtdIns*P* 3-kinase inhibition [8, 11]. Thus, accumulation of MTM1 substrates may play a key role in the altered SR Ca^{2+} release and associated muscle weakness.

In the present work, we aimed at further characterizing the pathophysiological features of the SR Ca^{2+} release process of MTM1-deficent muscle fibers at rest and during EC coupling. Our results demonstrate that the Ca^{2+}-gated activation mode of RYR channels is promoted under both conditions.

2. Methods

2.1 Preparation of the muscle fibers

All experiments and procedures were in accordance with the guidelines of the local animal ethics committee of the University Claude Bernard - Lyon 1, the French Ministry of Agriculture (decree 87/848) and the revised European Directive 2010/63/EU.

We used 4-5-week old wild type (WT) and *Mtm1*-KO male mice in the 129PAS background [6]. Single fibers were isolated from the *flexor digitorum brevis* (FDB) and interosseus muscles following previously described procedures [12]. In brief, mice were anaesthetized with isoflurane and killed by cervical dislocation. Muscles were removed and incubated for 60 minutes at 37 °C in the presence of external Tyrode containing 2 $mg.mL^{-1}$ collagenase (Sigma, type 1). Single fibers were obtained by triturating the collagenase-treated muscles within the experimental chamber consisting of a 50-mm-wide culture µ-dish (Ibidi GmbH, Martinsried, Germany). Measurements of Ca^{2+} sparks were carried out on muscle fibers isolated from FDB muscles from 5 WT and 5 *Mtm1*-KO mice. All experiments were performed at room temperature (20-22 °C).

2.2 Electrophysiology

We used the silicone voltage-clamp technique [12, 13]. For this, single fibers were partly insulated with silicone grease so that only a short portion (50-100 µm long) of the fiber extremity remained out of the silicone. Voltage-clamp was achieved with a micropipette filled with a solution mimicking the ionic composition of the cytosolic compartment and also containing the fluorescent Ca^{2+}-sensitive dye rhod-2 and a high concentration of EGTA (see Solutions). The tip of the micropipette was inserted through the silicone, within the insulated part of the fiber. The tip was gently crushed against the bottom of the chamber in order to ease intracellular equilibration and decrease series resistance. The chlorided silver wire inside the pipette was connected to an RK-400 patch-clamp amplifier (Bio-Logic, Claix, France) used in whole-cell voltage-clamp configuration, in combination with an analog-digital converter (Digidata 1440A, Axon Instruments, Foster City, CA) controlled by pClamp 9 software (Axon Instruments). Analog compensation was adjusted to further decrease the effective series resistance. Intracellular equilibration of the solution was allowed for a period of 30 min before initiating measurements. Membrane depolarizing steps of 0.5 s duration were applied from a holding command potential of -80 mV.

2.3 Confocal imaging

Confocal imaging was conducted with a Zeiss LSM 5 Exciter microscope equipped with a 63× oil immersion objective (numerical aperture 1.4). For measurements of voltage-activated Ca^{2+} transients in the presence of high intracellular EGTA we used the dye rhod-2: excitation was from the 543 nm line of a HeNe laser and fluorescence was collected above 560 nm. Rhod-2 Ca^{2+} transients were imaged using the line-scan mode (x,t) of the system with the line parallel to the

longitudinal axis of the fibers. Images were taken with a scanning frequency of 1.15 ms per line. Rhod-2 fluorescence changes were expressed as F/F_0 where F_0 is the baseline fluorescence. For Ca^{2+} sparks measurements, isolated muscle fibers were incubated for 30 minutes in the presence of Tyrode solution containing 10 µM fluo-4 AM. Fluo-4 fluorescence was detected above 505 nm upon excitation with the 488 nm line of an Argon laser. Fluo-4 fluorescence imaging was performed with either the *x,y* or the *x,t* scanning mode of the microscope.

2.4 Ca^{2+} release calculation

The SR Ca^{2+} release flux activated by membrane depolarization was estimated from the time derivative of the total myoplasmic Ca^{2+} ($[Ca_{Tot}]$) calculated from the occupancy of intracellular calcium binding sites according to a previously described procedure [14, 15]. For this, changes in $[Ca^{2+}]$ were calculated from the rhod-2 signals assuming a basal $[Ca^{2+}]$ of 0.1 µM and a Kd of rhod-2 for Ca^{2+} of 1.2 µM. The model included troponin C (TN) binding sites, parvalbumin binding sites and calcium transport across the SR membrane with the same parameters as used in [15]. Ca^{2+}-binding sites on EGTA make the major contribution with a total sites concentration of 6 mM, an "on" rate constant $k_{on,\ EGTA}$ of 0.056 $\mu M^{-1}.ms^{-1}$ and an "off" rate constant $k_{off,\ EGTA}$ of 0.002 ms^{-1}.

2.5 Ca^{2+} sparks analysis

Analysis was carried out according to previously described procedures [16, 17]. In brief, the region of the fiber and the background was defined on the first image of each *x,y* image series. The averaged background fluorescence was subtracted from each pixel of all images in one series. The calcium release events were detected by the stationary wavelet method. The filtering was made by soft thresholding wavelet detection. Finally the amplitude and full width at half

maximum (FWHM) of the sparks was calculated. Two FWHM values were calculated: perpendicular and parallel with the Z-lines. In order to detect the Z-lines, the frequency spectrum in each line of all images was calculated using fast Fourier transform. Finally inverse FFT of the frequency components corresponding to sarcomeres were used to remove the Z-lines from the images. The analysis of line-scan images was performed with an automatic event detection program [17], which calculated the amplitude (F/F_0), full width at half maximum (FWHM), duration and full time at half maximum (FTHM) of the identified events. Signal mass (SM) was calculated from the amplitudes and FWHM obtained by fitting the spatial profile of the events at every time point [18]. In order to describe the spatial profile of the events, the kurtosis (as defined in statistical mathematics and introduced for calcium sparks by Zhou et al. [19]) was used. Accordingly, a calcium release event was defined as "protoplatykurtic" if it had a flat top right from the first scan detection. The speed of spatial spread of activation was calculated from sequentially activating clusters of RYRs using the angle of the wave-front of propagation of the Ca^{2+} signal, as described earlier [20].

2.6 Solutions

Tyrode solution contained (in mM): 140 NaCl, 5 KCl, 2.5 $CaCl_2$, 2 $MgCl_2$, 10 Hepes. The extracellular solution used for voltage-clamp contained (in mM) 140 TEA-methanesulfonate, 2.5 $CaCl_2$, 2 $MgCl_2$, 1 4-aminopyridine, 10 HEPES and 0.002 tetrodotoxin. The pipette solution contained (in mM) 120 K-glutamate, 5 Na_2-ATP, 5 Na_2-phosphocreatine, 5.5 $MgCl_2$, 12 EGTA, 4.8 $CaCl_2$, 0.1 rhod-2, 5 glucose, 5 HEPES. Fluo-4 AM was dissolved and stored in DMSO. All solutions were adjusted to pH 7.20.

2.7 Statistics

Statistical analysis was performed with Origin 8.0 and GraphPad Prism 6. Unless otherwise specified, data values are presented as means ± S.E.M. for n fibers. For datasets passing the D'Agostino & Pearson omnibus normality test, statistical significance was determined using a Student's t-test (*p≤0.05, **p≤0.01, ***p≤0.001). Otherwise Mann Whitney test was applied to assess statistical significance.

3. Results

3.1 Kinetic alterations of voltage-activated SR Ca^{2+} release in MTM1-deficient muscle fibers

Figure 1 shows a collection of representative line-scan F/F_0 rhod-2 Ca^{2+} transients (top images) and of the corresponding calculated Ca^{2+} release fluxes (bottom images) triggered by voltage-clamp depolarization from -80 mV to -20, -10 and +10 mV, in 3 WT muscle fibers (A-C) and 3 MTM1-deficient muscle fibers (D-F). Experiments were performed in the presence of 12 mM EGTA to prevent contraction and to simplify Ca^{2+} release calculation. In each fiber, the 3 images were taken at the same Z level with the line positioned parallel at three nearby locations along the transverse axis. For the Ca^{2+} release flux calculation, images were compressed by averaging 10 consecutive rows along the line. The trace below each pair of F/F_0 and corresponding Ca^{2+} release flux images shows the time-course of Ca^{2+} release flux averaged over the entire scanned line.

Ca^{2+} release in WT fibers exhibits stereotyped kinetics, homogeneous along the line, characterized by an early peak, the amplitude of which increases with the pulse, followed by a decay that becomes faster as the peak amplitude gets larger. In MTM1-deficient muscle fibers,

we previously reported that voltage-activated Ca^{2+} release exhibits slow onset, reduced peak amplitude and reduced spatial synchrony [8]. Data in Fig. 1 (D-E) illustrates the fact that Ca^{2+} release in the diseased fibers also exhibits specifically marked kinetic alterations at voltage levels near -10 mV. In the example shown in Fig. 1D, Ca^{2+} release triggered by the pulse to -20 mV is heterogeneous along the line, with the top region yielding almost no change at the onset of the pulse as compared to the bottom region of the line. Later during that same pulse, a secondary phase of Ca^{2+} release appears to propagate from the bottom towards the top region of the line, so that within the line region pointed by the red arrow, peak Ca^{2+} release occurs after the end of the pulse (superimposed red Ca^{2+} release trace at the bottom). In the same fiber, upon depolarization to -10 mV (Fig. 1D, middle panel), a delayed release of Ca^{2+} occurs within the same line region, but earlier in time, during the pulse. For the largest pulse, some discrepancy persisted in terms of time to peak Ca^{2+} release between the top and bottom of the line, but to a much more reduced extent.

Severe spatial non-uniformity of Ca^{2+} release as illustrated in Fig. 1D, was not prerequisite to observe the occurrence of a delayed phase of Ca^{2+} release at intermediate activation voltages. This is illustrated in Fig. 1 E-F which shows that, despite reasonable uniformity along the line at the onset of the pulse, Ca^{2+} release was specifically prolonged and tended to exhibit a secondary delayed peak during the pulse to -10 mV. In contrast, during the pulses to -20 and +10 mV global Ca^{2+} release kinetics, although slower, were qualitatively similar to those in WT fibers.

Figure 2A shows the mean (± S.D., grey shading) Ca^{2+} release flux in WT and MTM1-deficient muscle fibers triggered by 500-ms long depolarizing pulses from -80 mV to values ranging between -20 and +20 mV. Mean traces were calculated from line-averaged rhod-2 *x,t* images collected from 20 and 13 fibers, issued from 5 and 5 WT and *Mtm1*-KO mice, respectively. Each

of the traces in the two conditions is shown with the *y* scale bar adjusted for best-viewing the time-course of the release flux at each voltage. *y* scale bars of identical length correspond to 3 times lower amplitude in the disease (KO) as compared to the WT condition. The early sharp peak of SR Ca^{2+} release at the onset of the pulse is lost in the MTM1-deficient muscle fibers and the overall time during which Ca^{2+} release remains elevated during the pulses is prolonged. This prolongation was not related to the lower peak amplitude of Ca^{2+} release, as illustrated in Fig. 2B which shows the superimposed mean Ca^{2+} release traces in response to a pulse to -20 mV in WT fibers and in response to a pulse to 0 mV in the MTM1-deficient fibers. Despite a larger peak amplitude in the disease condition, the time-course of Ca^{2+} release was clearly prolonged as compared to that in the WT condition.

The extent of peak Ca^{2+} release duration was estimated by measuring the half-width of the peak in the two groups of fibers. Mean values are reported *versus* membrane voltage in Fig. 2C. The mean value for MTM1-deficient fibers at -30 mV is not presented because Ca^{2+} release was too small and never exhibited an identifiable peak at this voltage so that the half-width would simply correspond to the pulse duration. Nevertheless, values for half-width were significantly larger in MTM1-deficient fibers as compared to WT fibers at all voltages, the difference being the largest at -20 and -10 mV. In fact, the mean half-width in MTM1-deficient fibers in response to a pulse to +20 mV was significantly larger than that in WT fibers in response to pulses ranging between -10 and +20 mV. This representation does not take into account the fact that the peak amplitude of Ca^{2+} release is smaller in MTM1-deficient fibers than in WT fibers at all voltages [8]. Figure 2D presents how the half-width of peak Ca^{2+} release depends on its amplitude for all records. In both groups of fibers the half-width decreases as the peak amplitude of Ca^{2+} release gets larger, with values reaching a minimum level near ~20 ms for the largest values of peak amplitude. However,

for peak values between 10 and 30 $\mu M.ms^{-1}$, corresponding values for half-width were, on average, close to or more than 2 times larger in MTM1-deficient fibers than in WT ones. This is best viewed in the inset of Fig. 2D where half-width values were binned and averaged according to their corresponding peak Ca^{2+} release amplitude, with an increment of 10 $\mu M.ms^{-1}$. For the lowest range of peak amplitudes (0-10 $\mu M.ms^{-1}$), half-width values from traces that did not exhibit an identifiable peak were excluded. These results demonstrate that despite slowing the onset and reducing the amplitude of the early peak level of RYR1-mediated Ca^{2+} release, MTM1 deficiency promotes RYR1channels activity over a more prolonged period of time following membrane depolarization at intermediate levels of activation.

3.2 Spontaneous local Ca^{2+} release events at rest in Mtm1-KO muscle fibers

Prolongation of voltage-activated Ca^{2+} release together with recurrent presence of an associated delayed rising phase during the depolarizing pulse (Fig. 1E) and/or of propagating events (Fig. 1D) suggest that RYR1 channels gating in the diseased fibers tends to get deprived from normal control by the t-tubule $Ca_V1.1$ voltage-sensors, a condition under which they may become activated by Ca^{2+} (see [4]). A now classical functional correlate of $Ca_V1.1$-free RYR1 channels in muscle is the presence of spatially localized Ca^{2+} release events taking the form of Ca^{2+} sparks [3, 4]. We thus looked for such events in intact WT and MTM1-deficient muscle fibers using the dye fluo-4 in the absence of any exogenous Ca^{2+} buffer. The left and right bottom panels in Fig. 3 show the standard deviation of fluo-4 fluorescence intensity over a series of 20 consecutive confocal frames at a given location of a WT and of an MTM1-deficient muscle fiber, respectively. For this, the mean and standard deviation of intensity at each pixel location were calculated. While the WT fiber was basically silent, fluorescence from the MTM1-deficient fiber exhibited local areas of large standard deviation, corresponding to presence of Ca^{2+} release

events. Figure 4 depicts the spatial properties of the events detected in MTM1-deficient fibers using *x,y* confocal laser scanning. Figure 4A shows one typical Ca^{2+} release event visualized as F/F_0 within an MTM1-deficient fiber, while an enlarged view of this same event is shown in Fig. 4B, together with its spatial profiles at the positions indicated by the arrows. This event exhibited a peak amplitude of ~$3F_0$ and expanded along both the longitudinal and transversal axis of the fiber with a half-width of approximately 2 µm. Figure 4C shows the frequency histogram of amplitude of the sparks detected in MTM1-deficient fibers while Fig. 4D shows the histograms of full width at half-maximum (FWHM) for profiles parallel (X) and perpendicular (Y) to the fiber axis. Data are from 2485 events detected from 51 fibers from 5 *Mtm1*-KO mice, respectively. In comparison, 34 events were detected from 45 fibers from 5 WT mice, respectively, the mean amplitude and FWMH of which are indicated with arrows in the histograms of Fig. 4C-D. Table 1 reports mean values for peak amplitude, FWMH and frequency for events detected in WT and MTM1-deficient muscle fibers. For this, only events exhibiting peak amplitude comprised between 0.2 and 10 F/F_0, and FWHM comprised between 0.4 and 10 µm, were selected (34 events from 43 WT fibers and 1008 events from 51 MTM1-deficient fibers). MTM1-deficient fibers yielded events at a frequency more than 20 times that in WT fibers. Mean values for peak amplitude and FWHM along the transverse axis did not differ between the two groups, whereas the FWHM along the longitudinal axis was significantly larger, by ~25 %, in the diseased fibers.

The amplitude and spatial features of these Ca^{2+} release events are similar to those of the events that can be detected in saponin-permeabilized muscle fibers, a condition that disrupts the $Ca_V1.1$-RYR1 interaction (e.g. [21]). In contrast to the WT situation, Ca^{2+} release events in intact MTM1-deficient fibers were frequent enough to be easily captured under line-scan imaging

configuration. This is illustrated in Fig. 5 which shows typical examples of the spatio-temporal features of the events present in the diseased fibers. They were either lone short events exhibiting features of archetypical Ca^{2+} sparks (Fig. 5A) or series of such Ca^{2+} sparks or long-lasting events of lower amplitude and long duration commonly referred to as Ca^{2+} embers (Fig. 5B, see [3]). Amplitude and FWMH histograms for the lone Ca^{2+} sparks are shown in Fig.5C and 5D, respectively. Data are from 842 events collected from 38 muscle fibers isolated from 3 mice, respectively. Corresponding mean values for amplitude, rise-time, FWHM, FTHM and duration were 1.18 ± 0.02 F/F_0, 9.4 ± 0.2 ms, 1.71 ± 0.03 μm, 12.7 ± 0.2 ms and 28.6 ± 0.4 ms, respectively.

Figure 5E shows the distribution of events frequency in individual line-scan images. The superimposed line presents the theoretical Poisson-distribution ($\lambda = 3.99$) based on the assumption that the events occur independently of one another, while the inset shows an enlarged part of the graph to emphasize the presence of unexpectedly large number of events on certain images. These results indicate that Ca^{2+} release events did not appear randomly but were more frequent in particular locations of the diseased muscle fibers, suggesting that they did not simply result from uniformly altered RYR1 channel gating.

In Fig.6, we calculated the time-course of calcium release from the SR during lone Ca^{2+} sparks (right panels) and during a repeated series of such events (left panels). The time course of the amount of calcium released was derived as that of the Signal Mass (SM, Fig. 6C and G), calculated from the amplitudes and FWHM obtained by fitting the spatial profile of the events at every time point (for further details see Methods). Fig. 6D and H show the time derivative of SM (d(SM)/dt) representing the time course of SR calcium release flux. Note that in case of the large event presented in Fig. 6A, the hypothetical wrap curve over the individual peaks would follow the same time course as the global release does (see e.g. Fig. 2A), namely, after the rise to an

early peak it declines to a maintained steady level. This finding is in line with the expectation that calcium-dependent inactivation of RYR1, if calcium release is maintained, occurs at the local level.

Strikingly, MTM1-deficient fibers were able to generate massive Ca^{2+} release events exhibiting unconventionally large amplitude and spatial width. These represented approximately 5 % of the total number of detected events (55 events from 18 fibers from 3 mice, Fig. 5D). One example is shown in Fig. 7A where the event displays peak amplitude larger than 4 F_0 and expands spatially over ~4 µm. Note that the spatial profile of the event is flat just 1.145 ms (i.e. one scanning line) after its onset. The presence of such protoplatycurtic events can only be explained if vast arrays of release channels are activated simultaneously. The distribution of FWHM of such events, selected on the basis of FWHM larger than 3.5 µm is presented in Fig. 7B, showing that approximately 20 % of these events yielded a FWHM larger than 5 µm. These included events of giant space-width, as illustrated in Fig. 7C, during which new fiber regions get recruited as time goes. As the spatial profile of the triggered events is also protoplatycurtic (as demonstrated by the $F(x)$ profiles of individual line-scans – 1, 3, …, 11 – into the event) these observations provide further evidence for Ca^{2+} release events triggering the instantaneous activation of large clusters of RYR1 channels. Furthermore they provide the possibility to estimate the speed of spreading of activation presumably via CICR. For the events presented in Fig. 7C this was calculated to be 170 µm/s. In 6 similar events the average speed was found to be 228 ± 47 µm/s. Thus, in this framework, the activation of calcium release channels within junctional clusters would involve intermolecular interactions and therefore appear as instantaneous in our line-scan images, while propagation between neighboring clusters would use CICR.

3.3 Ca^{2+}sparks do not make a critical contribution to voltage-activated SR Ca^{2+} release in MTM1-deficient muscle fibers

As compared to the above measurements of resting Ca^{2+} release activity performed with the dye fluo-4 in the absence of exogenous Ca^{2+} buffer, our analysis of voltage-activated SR Ca^{2+} release (Figs. 1-2) was conducted with the somewhat lower affinity dye rhod-2 in the presence of a large concentration of intracellular EGTA. As these conditions may either prevent or compromise triggering or detection of Ca^{2+} sparks, we took measurements of voltage-activated fluo-4 transients under non buffering conditions, in order to determine whether Ca^{2+} sparks would be mandatory contributors of voltage-activated SR Ca^{2+} release in the diseased fibers. For this, line-scan images of fluo-4 fluorescence were taken from 3 MTM1-deficient muscle fibers voltage-clamp-depolarized to levels that activated Ca^{2+} release without triggering contraction. As illustrated in Fig. 8, results provided no indication that Ca^{2+} sparks would be systematically associated with voltage-activated Ca^{2+} release in the diseased fibers, as it is the case in frog muscle fibers [22, 23].

4. Discussion

The present results show that MTM1-deficient fibers exhibit local spontaneous Ca^{2+} release events at rest and prolonged activity of RYR1 channels during the early phase of voltage-triggered SR Ca^{2+} release. Ca^{2+} release events are very similar to those observed under conditions promoting disruption of $Ca_V1.1$-RYR1 interaction [e.g. 21] and consequent liberty for RYR1s to be gated by Ca^{2+} and to be responsible for Ca^{2+}-induced SR Ca^{2+} release. Accordingly, previous

indication that Ca^{2+}-induced Ca^{2+} release also operates during SR Ca^{2+} release activated by t-tubule depolarization [8] is the very likely the reason for the conspicuous alteration of the release flux kinetics.

There is evidence so far that CICR contributes to physiological Ca^{2+} release in muscles containing a substantial fraction of type 3 isoform of ryanodine receptor (RYR3). As compared to RYR1 channels which occupy the junctional SR membrane and directly face Cav1.1 voltage sensors in the t-tubule membrane, RYR3 channels are believed to reside in a parajunctional position [24], making them unlikely to be activated through a mechanism other than Ca^{2+} gating. The presence of CICR in RYR3-containing muscle was proposed on the basis of specific differences in the kinetic properties of voltage-triggered SR Ca^{2+} release in frog as compared to rat muscle [25], and on kinetic changes observed when frog fibers were challenged by experimental conditions expected to affect CICR, including the presence of various types of Ca^{2+} buffers (see [25-28]). CICR in RYR3-containing muscle was confirmed by the discovery of spontaneous Ca^{2+} sparks at rest [23, 29] and by contribution of these events to SR Ca^{2+} release during EC coupling [22, 23] (see for review [3, 4]).

In contrast, differentiated mammalian muscle contains a negligible proportion of RYR3, and, in coherence, several lines of results tend to exclude contribution of CICR to physiological EC coupling in this tissue [25, 30] including absence of Ca^{2+} sparks at rest and during activation. Still, spontaneous Ca^{2+} sparks are triggered in mammalian muscle under conditions believed to disrupt the $Ca_V1.1$-RYR1 interaction, including osmotic changes and t-tubule membrane permeabilization [31, 32]. This indicates that RYR1 channels in differentiated muscle fibers can also be gated open by Ca^{2+} when they are free of the $Ca_V1.1$ control. This could explain the presence of Ca^{2+} sparks at rest in MTM1-deficient muscle fibers. Indeed, in line with our analysis showing that spatial distribution of these events is not random (Fig. 5E) one simple explanation

could be that their occurrence spatially correlates with previously described local regions of t-tubule disruption [7, 8] and that occasionally observed massive Ca^{2+} release events (Fig. 7) would correspond to RYR1 channels operating within fiber regions yielding extensive loss of t-tubule network. However, there may be as well other parameters either determining or contributing to occurrence of Ca^{2+} sparks in this model. As an example, records in Fig. 8 show that spontaneous Ca^{2+}release can occur at rest within a fiber region where voltage-activated Ca^{2+} release is working and thus where t-tubule structure was preserved. There thus has to be alternative possible explanations for the occurrence of spontaneous Ca^{2+} release events in MTM1-deficient fibers. We previously showed that MTM1 substrates loaded into normal muscle fibers depress voltage-activated Ca^{2+} release and depress the frequency of Ca^{2+} sparks triggered by permeabilization [21]. Along this line, it could be speculated that MTM1 substrates accumulation is spatially heterogeneous in MTM1-deficient fibers so that areas devoid of Ca^{2+} sparks would actually correspond to regions where substrates have accumulated the most and prevent RYR1 channel opening.

In this same context it is also worth emphasizing that muscle fibers from another mouse model of centronuclear myopathy, due to a mutation in the *Dnm2* gene, also exhibit spontaneous Ca^{2+} sparks at rest [33]. However, one major difference between the two models is that *Dnm2* disease fibers exhibit no stringent alterations of the t-tubule network [33] as was observed in MTM1-deficient muscle fibers. Still, considering the close links between MTM1 and DNM2 (see for instance [34]), it is tempting to assume that muscle fibers from the two corresponding disease mouse models share a common mechanism contributing to spontaneous activity of RYR1 channels under the form of Ca^{2+} sparks, independent from t-tubule alterations. In this framework, the fact that sparks frequency in MTM1-deficient fibers is only approximately twice that in *Dnm2* disease fibers further supports the postulate that, despite no apparent disruption of the t-tubule

network, $Ca_V1.1$ control of RYR1 channels is substantially loosened in that particular disease condition too [33].

At last, it is worth stressing that the situation in MTM1-deficient fibers remains very much distinct from that of RYR3-containing intact muscle fibers. Indeed, although we cannot exclude that extensive series of measurements in MTM1-deficient fibers could have revealed the occasional presence of Ca^{2+} sparks during a depolarizing pulse, these events are not mandatory contributors of voltage-activated SR Ca^{2+} release (Fig.8) as they are for instance in frog muscle fibers [22, 23].

We previously reported that, when measuring Ca^{2+} release under high-EGTA buffering conditions, MTM1-deficient muscle fibers tend to exhibit a delayed phase of Ca^{2+} release onset during depolarizing pulses at intermediate voltages [8], consistent with opening of RYR1 channels triggered when a threshold Ca^{2+} level is reached. Our present analysis now shows that, in these conditions, the early peak phase of SR Ca^{2+} release lasts longer in MTM1-deficient fibers than in WT fibers, at all levels of membrane voltage activation. This occurs even under conditions when Ca^{2+} release is well synchronized all along the scanned line (e.g. Fig. 1F), a situation that excludes severely altered t-tubule network at specific locations of the line. Such difference does not exist between the time-course of voltage-triggered SR Ca^{2+} release in frog and mammals [25], which further supports the dissimilarity between properties of Ca^{2+} release exhibiting CICR contribution in RYR3-containing healthy muscle and Ca^{2+} release alterations in the present disease situation. The increased half-duration of peak Ca^{2+} release in MTM1-deficient fibers reveals that RYR1 channels (or some RYR1 channels) remain open for a prolonged period of time during an activating voltage pulse. An intuitive explanation would be that enhanced propensity for generation of a Ca^{2+}-activated component of Ca^{2+}release at late times during a depolarizing pulse is responsible for this. However, a simple simulation assuming a late

component of Ca^{2+} release with properties described previously (peak rate of 3 µM.ms^{-1}, [8]) occurring at random times during a pulse, failed to reproduce the prolonged time-course of Ca^{2+} release observed in MTM1-deficient fibers (not illustrated). One possibility then is that a particular combination of $Ca_V1.1$ controlled RYR1 channels, of $Ca_V1.1$-free RYR1 channels capable of CICR and of non-functional or lost RYR1 channels is necessary to generate the kinetic features of Ca^{2+} release observed here. Future efforts, including mathematical modelling of such combinations may prove able to reproduce the entire kinetic alterations of Ca^{2+} release in MTM1-deficient muscle fibers and to also provide further insights into our understanding of this disease situation with impact for our understanding of normal Ca^{2+} release function.

As for the question of how MTM1 is compulsory for proper function of $Ca_V1.1$-RYR1 coupling, it still remains ambiguous and as discussed earlier, may involve mechanisms involved both in proper maintenance of t-tubule membrane and triad organization and also directly in RYR1 channel function [8, 21, 33, 34]. In the present context, both may play a role in the promotion of Ca^{2+}-induced Ca^{2+} release because, on the one hand, of loss or loosened control of RYR1 by $Ca_V1.1$ due to triad membrane architecture defects and, on the other hand, of perturbed RYR1 function due to altered availability of MTM1 phosphoinositide substrates and/or products having a regulatory role on the channel activity.

Finally, it is interesting to speculate about the physiological relevance of CICR under MTM1-defciency as well as in analogous disease conditions. Indeed, one may simply picture CICR contribution to Ca^{2+} homeostasis as a collateral consequence of RYR1 channels uncoupling from the t-tubule voltage control, with no specific biological relevance to muscle function. However, one may also consider that the capacity of RYR1 to be gated by Ca^{2+} under conditions when it loses its normal control, grants the muscle fibers with an alternative compensatory mechanism to help sustain EC coupling under such distress situations. Importantly,

disruption of the t-tubule network in MTM1-deficient fibers is clearly not accompanied by complete collapse of fiber structure and SR compartment because RYR1 channels are still active in this membrane, capable of generating cytosolic Ca^{2+} changes witnessing a maintained luminal SR content. Nevertheless, this is obviously not sufficient to maintain proper muscle function in myotubular myopathy because the eventual extensive disruption of the t-tubule network precludes any possibility for Ca^{2+} to be raised at sufficient high level to activate contraction throughout the entire cross-section of the fibers. Nevertheless, we propose that Ca^{2+}-gated RYR1 channels contribution to Ca^{2+} release may help sustain muscle function in analogous milder pathological situations. Conversely however, it is undeniable that widespread occurrence of Ca^{2+}-induced Ca^{2+} release will generate uncoordinated Ca^{2+} signals that will be of little help for muscle fiber contractile function. In that case they may instead cause a host of undesired secondary problems adding up to the disease phenotype.

Conclusions

Deficient SR Ca^{2+} release is a key determinant of muscle weakness in myotubular myopathy. SR Ca^{2+} release in this disease situation is not only depressed in amplitude but the underlying molecular mechanism substantially differs from the one in healthy muscle as MTM1-deficient fibers exhibit a contribution from Ca^{2+}-gated ryanodine receptors at rest and during EC coupling.

Contributors

All experiments were performed at Institut NeuroMyoGène, University Claude Bernard, Lyon 1. VJ designed the study. AB-B designed and generated the Mtm1-KO mouse model. CK and VJ performed the electrophysiological and confocal imaging experiments. PS and LC performed the Ca^{2+} sparks analysis. CK, PS, BA, AB-B, LC and VJ contributed to data interpretation and discussion and to critical revisions of the manuscript.

Declarations of interest

None.

Funding sources

This work was supported by grants from CNRS, INSERM and Université Claude Bernard - Lyon 1 to Institut NeuroMyoGène. This work was also supported by the Association Française contre les Myopathies (AFM-Téléthon: Alliance MyoNeurALP program; project 5.3.4.4 to V. Jacquemond), by grants to L. Csernoch from the Hungarian National Research, Development and Innovation Office (NKFIH K-115461) and from the GINOP-2.3.2-15-2016-00040 project, and by a grant to C. Kutchukian from the Société Française de Myologie (SFM). None of the funding sources had a role in study design, in the collection, analysis and interpretation of data, in the writing of the report. Decision to submit the article for publication was approved by the MyoNeurAlp program.

References

1. E. Ríos, G. Pizarro, E. Stefani, Charge movement and the nature of signal transduction in skeletal muscle excitation-contraction coupling, Annu Rev Physiol. 54 (1992) 109-133.

2. M.F. Schneider, Control of calcium release in functioning skeletal muscle fibers, Annu Rev Physiol. 56 (1994) 463-484.

3. L. Csernoch, Sparks and embers of skeletal muscle: the exciting events of contractile activation, Pflugers Arch. 454 (2007) 869-878.

4. E. Ríos, Calcium-induced release of calcium in muscle: 50 years of work and the emerging consensus, J Gen Physiol.150 (2018) 521-537.

5. J. Laporte, L.J. Hu, C. Kretz, J.L. Mandel, P. Kioschis, J.F. Coy, S.M. Klauck, A. Poustka, N. Dahl, A gene mutated in X-linked myotubular myopathy defines a new putative tyrosine phosphatase family conserved in yeast, Nat Genet. 13 (1996) 175-182.

6. A. Buj-Bello, V. Laugel, N. Messaddeq, H. Zahreddine, J. Laporte, J.F. Pellissier, J.L. Mandel, The lipid phosphatase myotubularin is essential for skeletal muscle maintenance but not for myogenesis in mice, Proc Natl Acad Sci USA. 99 (2002) 15060-15065.

7. L. Al-Qusairi, N. Weiss, A. Toussaint, C. Berbey, N. Messaddeq, C. Kretz, D. Sanoudou, A.H. Beggs, B. Allard, J.L. Mandel, J. Laporte, V. Jacquemond, A. Buj-Bello, T-tubule

disorganization and defective excitation-contraction coupling in muscle fibers lacking myotubularin lipid phosphatase, Proc Natl Acad Sci USA. 106 (2009) 18763-18768

8. C. Kutchukian, M. Lo Scrudato, Y. Tourneur, K. Poulard, A. Vignaud, C. Berthier, B. Allard, M.W. Lawlor, A. Buj-Bello, V. Jacquemond, Phosphatidylinositol 3-kinase inhibition restores Ca^{2+} release defects and prolongs survival in myotubularin-deficient mice, Proc Natl Acad Sci USA. 113 (2016) 14432-14437.

9. G.S. Taylor, T. Maehama, J.E. Dixon, Myotubularin, a protein tyrosine phosphatase mutated in myotubular myopathy, dephosphorylates the lipid second messenger, phosphatidylinositol 3-phosphate, Proc Natl Acad Sci USA. 97 (2009) 8910-8915.

10. H. Tronchère, J. Laporte, C. Pendaries, C. Chaussade, L. Liaubet, L. Pirola, J.L. Mandel, B. Payrastre, Production of phosphatidylinositol 5-phosphate by the phosphoinositide 3-phosphatase myotubularin in mammalian cells, J Biol Chem.279 (2004) 7304-7312.

11. N. Sabha, J.R. Volpatti, H. Gonorazky, A. Reifler, A.E. Davidson, X. Li, N.M. Eltayeb, C. Dall'Armi, G. Di Paolo, S.V. Brooks, A. Buj-Bello, E.L. Feldman, J.J. Dowling, PIK3C2B inhibition improves function and prolongs survival in myotubular myopathy animal models, J Clin Invest.126 (2016) 3613-3625.

12. V. Jacquemond, Indo-1 fluorescence signals elicited by membrane depolarization in enzymatically isolated mouse skeletal muscle fibers, Biophys J. 73 (1997) 920-928.

13. R. Lefebvre, S. Pouvreau, C. Collet, B. Allard, V. Jacquemond, Whole-cell voltage clamp on skeletal muscle fibers with the silicone-clamp technique, Methods Mol Biol. 1183 (2014) 159-170.

14. S. Pouvreau, L. Csernoch, B. Allard, J.M. Sabatier, M. De Waard, M. Ronjat, V. Jacquemond, Transient loss of voltage control of Ca^{2+} release in the presence of maurocalcine in skeletal muscle, Biophys J. 91 (2006) 2206-2215.

15. R. Lefebvre, C. Legrand, E. González-Rodríguez, L. Groom, R.T. Dirksen, V. Jacquemond, Defects in Ca^{2+} release associated with local expression of pathological ryanodine receptors in mouse muscle fibres, J Physiol. 589 (2011) 5361-5382.

16. L. Csernoch, S. Pouvreau, M. Ronjat, V. Jacquemond, Voltage-activated elementary calcium release events in isolated mouse skeletal muscle fibers, J Membr Biol. 226 (2008) 43-55.

17. L.Z. Szabó, J. Vincze, L. Csernoch, P. Szentesi, Improved spark and ember detection using stationary wavelet transforms, J Theor Biol. 264 (2010) 1279-1292.

18. S. Hollingworth, J. Peet, W.K. Chandler, S.M. Baylor, Calcium sparks in intact skeletal muscle fibers of the frog, J Gen Physiol. 118 (2001) 653-678.

19. J. Zhou, G. Brum, A. González, B.S. Launikonis, M.D. Stern, E. Ríos, Concerted vs. sequential. Two activation patterns of vast arrays of intracellular Ca^{2+} channels in muscle, J Gen Physiol. 126 (2005) 301-309.

20. M. Sztretye, J. Almássy, T. Deli, P. Szentesi, C. Jung, B. Dienes, C.A. Simut, E. Niggli, I. Jona, L. Csernoch, Altered sarcoplasmic reticulum calcium transport in the presence of the heavy metal chelator TPEN, Cell Calcium 46 (2009) 347-355.

21. E.G. Rodríguez, R. Lefebvre, D. Bodnár, C. Legrand, P. Szentesi, J. Vincze, K. Poulard, J. Bertrand-Michel, L. Csernoch, A. Buj-Bello, V. Jacquemond, Phosphoinositide substrates of myotubularin affect voltage-activated Ca^{2+} release in skeletal muscle, Pflugers Arch. 466 (2014) 973-985.

22. A. Tsugorka, E. Ríos, L.A. Blatter, Imaging elementary events of calcium release in skeletal muscle cells, Science 269 (1995) 1723-1726.

23. M.G. Klein, H. Cheng, L.F. Santana, Y.H. Jiang, W.J. Lederer, M.F. Schneider, Two mechanisms of quantized calcium release in skeletal muscle, Nature 379 (1996) 455-458.

24. E. Felder, C. Franzini-Armstrong, Type 3 ryanodine receptors of skeletal muscle are segregated in a parajunctional position, Proc Natl Acad Sci USA. 99 (2002) 1695-1700.

25. N. Shirokova, J. García, G. Pizarro, E. Ríos, Ca^{2+} release from the sarcoplasmic reticulum compared in amphibian and mammalian skeletal muscle, J Gen Physiol. 107 (1996) 1-18.

26. V. Jacquemond, L. Csernoch, M.G. Klein, M.F. Schneider, Voltage-gated and calcium-gated calcium release during depolarization of skeletal muscle fibers, Biophys J. 60 (1991) 867-873.

27. L. Csernoch, V. Jacquemond, M.F. Schneider, Microinjection of strong calcium buffers suppresses the peak of calcium release during depolarization in frog skeletal muscle fibers, J Gen Physiol. 101 (1993) 297-333.

28. J.F. Olivera, G. Pizarro, A study of the mechanisms of excitation-contraction coupling in frog skeletal muscle based on measurements of [Ca^{2+}] transients inside the sarcoplasmic reticulum, J Muscle Res Cell Motil. 39 (2018) 41-60.

29. S. Perni, K.C. Marsden, M. Escobar, S. Hollingworth, S.M. Baylor, C. Franzini-Armstrong, Structural and functional properties of ryanodine receptor type 3 in zebrafish tail muscle, J Gen Physiol. 145 (2015) 173-184.

30. S. Hollingworth, S.M. Baylor, Comparison of myoplasmic calcium movements during excitation-contraction coupling in frog twitch and mouse fast-twitch muscle fibers, J Gen Physiol. 141 (2013) 567-583.

31. W.G. Kirsch, D. Uttenweiler, R.H. Fink, Spark- and ember-like elementary Ca^{2+} release events in skinned fibres of adult mammalian skeletal muscle, J Physiol. 537 (2001) 379-389.

32. X. Wang, N. Weisleder, C. Collet, J. Zhou, Y. Chu, Y. Hirata, X. Zhao, Z. Pan, M. Brotto, H. Cheng, J. Ma, Uncontrolled calcium sparks act as a dystrophic signal for mammalian skeletal muscle, Nat Cell Biol. 7 (2005) 525-530.

33. C. Kutchukian, P. Szentesi, B. Allard, D. Trochet, M. Beuvin, C. Berthier, Y. Tourneur, P. Guicheney, L. Csernoch, M. Bitoun, V. Jacquemond, Impaired excitation-contraction coupling in muscle fibres from the dynamin2R465W mouse model of centronuclear myopathy, J Physiol. 595 (2017) 7369-7382.

34. L. Csernoch, V. Jacquemond, Phosphoinositides in Ca^{2+} signaling and excitation-contraction coupling in skeletal muscle: an old player and newcomers, J Muscle Res Cell Motil. 36 (2015) 491-499.

Figures legends

Figure 1. *x,t* confocal imaging of voltage-activated SR Ca^{2+} release in WT and MTM1-deficient muscle fibers. *A-F*, line-scan image of rhod-2 fluorescence (top image) and of corresponding calculated Ca^{2+} release flux (bottom image) from 3 WT fibers (*A-C*) and 3 MTM1-deficient fibers (*D-F*) stimulated by the voltage clamp pulse shown on top. The trace below each pair of F/F_0 and Ca^{2+} release flux images in a given fiber stimulated by a given pulse corresponds to the average time-course of Ca^{2+} release calculated from the whole image. In *D*, the superimposed red trace shows the time course of Ca^{2+} release at the particular location of the scanned line marked by a red arrow in the corresponding Ca^{2+} release flux image.

Figure 2. Altered kinetic features of voltage-activated SR Ca^{2+} release in MTM1-deficient muscle fibers. *A*, mean ± S.D. (grey shading) time course of Ca^{2+} release flux in WT fibers (left, n=20) and MTM1-deficient fibers (right, n=13) in response to 500-ms long depolarizing pulses from -80 mV to the indicated values. *y* scale bars all correspond to 9 $\mu M.ms^{-1}$ and 3 $\mu M.ms^{-1}$ in the WT and MTM1-deficiency conditions, respectively. *B*, superimposed mean Ca^{2+} release flux evoked by a pulse to -20 mV in WT fibers (continuous trace) and in response to a pulse to 0 mV in MTM1-deficient fibers (dotted trace). *C*, dependence upon voltage of the mean ± S.E.M. half-width of peak Ca^{2+} release in WT fibers (closed bars) and in MTM1-deficient fibers (open bars). *D*, dependence of the half-width of Ca^{2+} release upon its peak amplitude in WT fibers (closed symbols) and MTM1-deficient fibers (open symbols). The inset in Fig. 2D presents mean values for half-width plotted *versus* corresponding mean values for peak amplitude. For this, pairs of peak amplitude/half-width values were sorted according to the peak amplitude. Values for half-

width falling within a same range of peak amplitude, following a 10 $\mu M.ms^{-1}$ increment, were then averaged and plotted versus the corresponding values for mean amplitude.

Figure 3. Ca^{2+} sparks in intact muscle fibers from *Mtm1-KO* mice. *x,y* images of the standard deviation of fluo-4 fluorescence intensity (bottom images) at each pixel position during a sequence of 20 successive frames taken from a WT fiber (left) and from an MTM1-deficient fiber (right). Corresponding transmitted light images of the two fibers are shown above. Note that the original images were resolved on 12 bit (0-4095).

Figure 4. Spatial features of Ca^{2+} sparks detected with *x,y* confocal imaging in muscle fibers from *Mtm1-KO* mice. *A*, *x,y* image of fluo-4 fluorescence from an intact isolated muscle fiber showing a local increase in Ca^{2+} visualized as the relative increase in fluorescence (F/F_0) after removing the structure elements and correcting for baseline fluorescence (F_0). *B*, enlarged view of the individual spark marked in panel *A*, together with spatial profiles of its amplitude calculated parallel (trace on the right) and perpendicular (trace below) to the main fiber axis at positions indicated by the arrows. Colour bar applies to both *A* and *B*. *C*, histogram of events amplitude. *D*, histograms of FWHM for profiles parallel (X) and perpendicular (Y) to the fiber axis. Arrows in *C* and *D* point to the corresponding mean values from the few events detected in WT fibers.

Figure 5. Spatio-temporal features of Ca^{2+} sparks detected using *x,t* confocal imaging in muscle fibers from *Mtm1-KO* mice. *A-B*, normalized line-scan images (F/F_0) of fluo-4 fluorescence from intact MTM1-deficient fibers showing typical calcium release events that are either lone calcium sparks (*A*) or a series of such events or long embers (*B*). Images shown at the

bottom show an enlarged portion of the arrow-pointed regions, displaying the individual events at increased temporal and spatial resolution together with their time course and spatial distribution. *C*, histogram of events amplitude. *D*, histograms of FWHM. *E*, distribution of the event frequencies in individual images. Continuous line presents the theoretical Poisson-distribution (λ = 3.99) based on the assumption that the events occur independently of one another. Inset shows an enlarged portion of the graph emphasizing the presence of unexpectedly large number of events in certain images.

Figure 6. Rate of SR Ca^{2+} release underlying Ca^{2+} sparks in muscle fibers from *Mtm1-KO* mice. *A*, *E* line-scan images of different types of Ca^{2+} release events corresponding to large (*A*) and small (*E*) repetitive calcium sparks. *B*, *F* corresponding temporal profile of F/F_0. *C, G* corresponding time course of the Signal Mass (SM), calculated from the values for amplitude and FWHM obtained by fitting the spatial profile of the events in *A* and *E* at every time point (for further details see Methods). *D, H* time derivative of SM (d(SM)/dt) representing the time course of calcium release flux from the SR.

Figure 7. Vast arrays of RYR1 channels can contribute to spontaneous Ca^{2+} release at rest in MTM1-deficient muscle fibers. *A*, individual protoplatycurtic Ca^{2+} spark with extremely large FWHM. Spatial and temporal profiles are presented next to and below the image, respectively. The several spatial profiles of fluorescence (from left to right) correspond to the one profiles right before the event and then during the 1st, 3rd, and 5th scan into the event (denoted as 0, 1, 3, and 5, respectively; corresponding to time points 0, 1.15, 3.45, and 5.75 ms, respectively). *B*, distribution of FWHM for Ca^{2+} release events with FWHM greater than 3.5 μm (n=55). *C*, Ca^{2+} release events trigger additional events in neighbouring clusters of ryanodine receptors. The

spatial profiles show the fluorescence right before and during the 1st, 3rd, 5th, 7th, and 11th scan into the event (denoted as 0, 1, 3, 5, 7, and 11, respectively; corresponding to time points 0, 1.15, 3.45, 5.75, 8.05, and 12.65 ms, respectively). Additional positions with an increase in Ca^{2+} appear as time progresses. Arrows in panels A and C above the images show the position of the first (black) and last (grey) scanlines the spatial profiles of which are displayed (in black and grey, respectively) next to the images. White arrow in panel C depicts the position where the speed of spreading of activation was calculated (170 µm/s for the event presented here).

Figure 8. Ca^{2+} sparks do not underlie voltage-activated SR Ca^{2+} release in MTM1-deficient fibers. Line-scan image of fluo-4 fluorescence from two distinct MTM1-deficient fibers (*A*, *B*) recorded while a voltage-clamp depolarizing pulse from -80 mV to the indicated value was applied.

Table 1:

Mean values for the spark parameters detected in *x,y* images.

	WT (n=34 events from 43 fibers)	***Mtm1*-KO (n=1008 events from 51 fibers)**
Peak amplitude (F/F_0)	1.01 ± 0.06	1.04 ± 0.02
FWHM-X (µm)	1.71 ± 0.08	2.15 ± 0.02 ***
FWHM-Y (µm)	1.67 ± 0.07	1.78 ± 0.02
Frequency ($Hz.mm^{-2}$)	11.9 ± 5.0	336.7 ± 53.4 ***

Fig.1

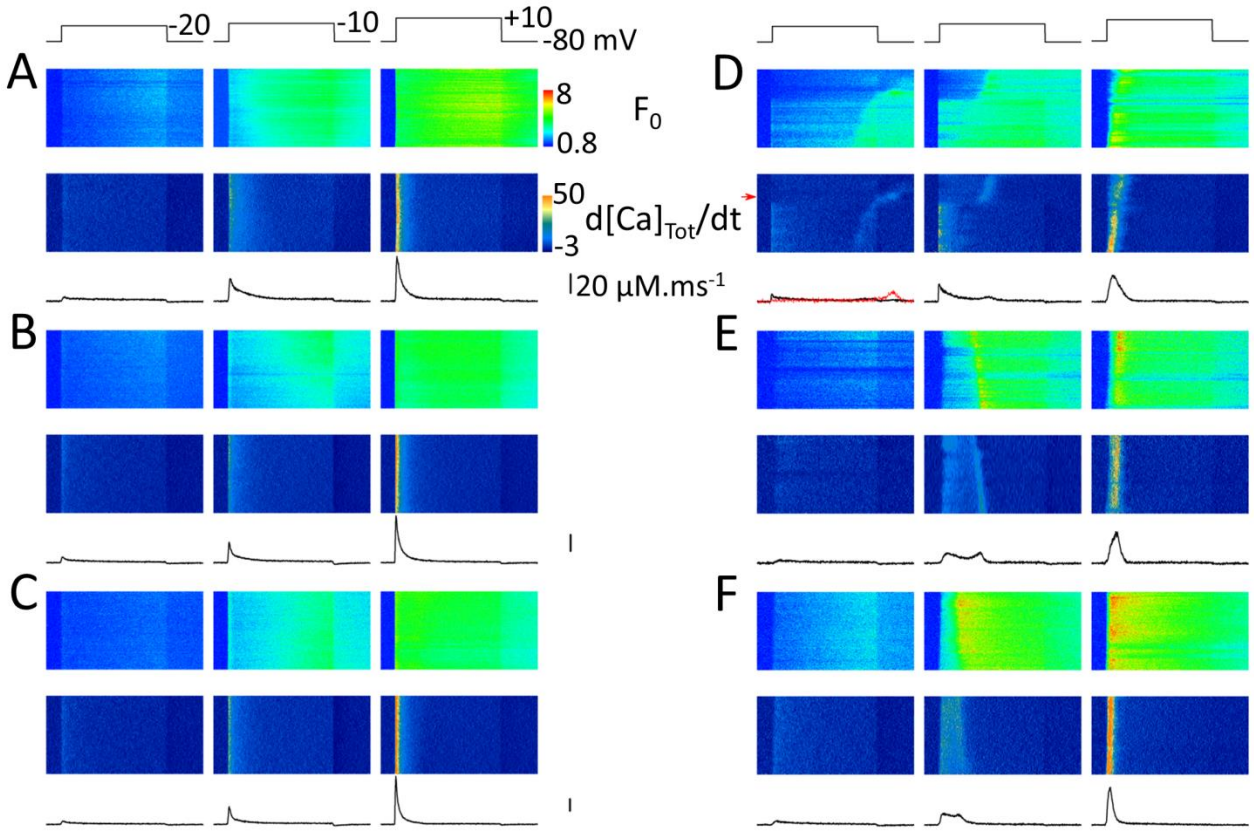

Fig.2

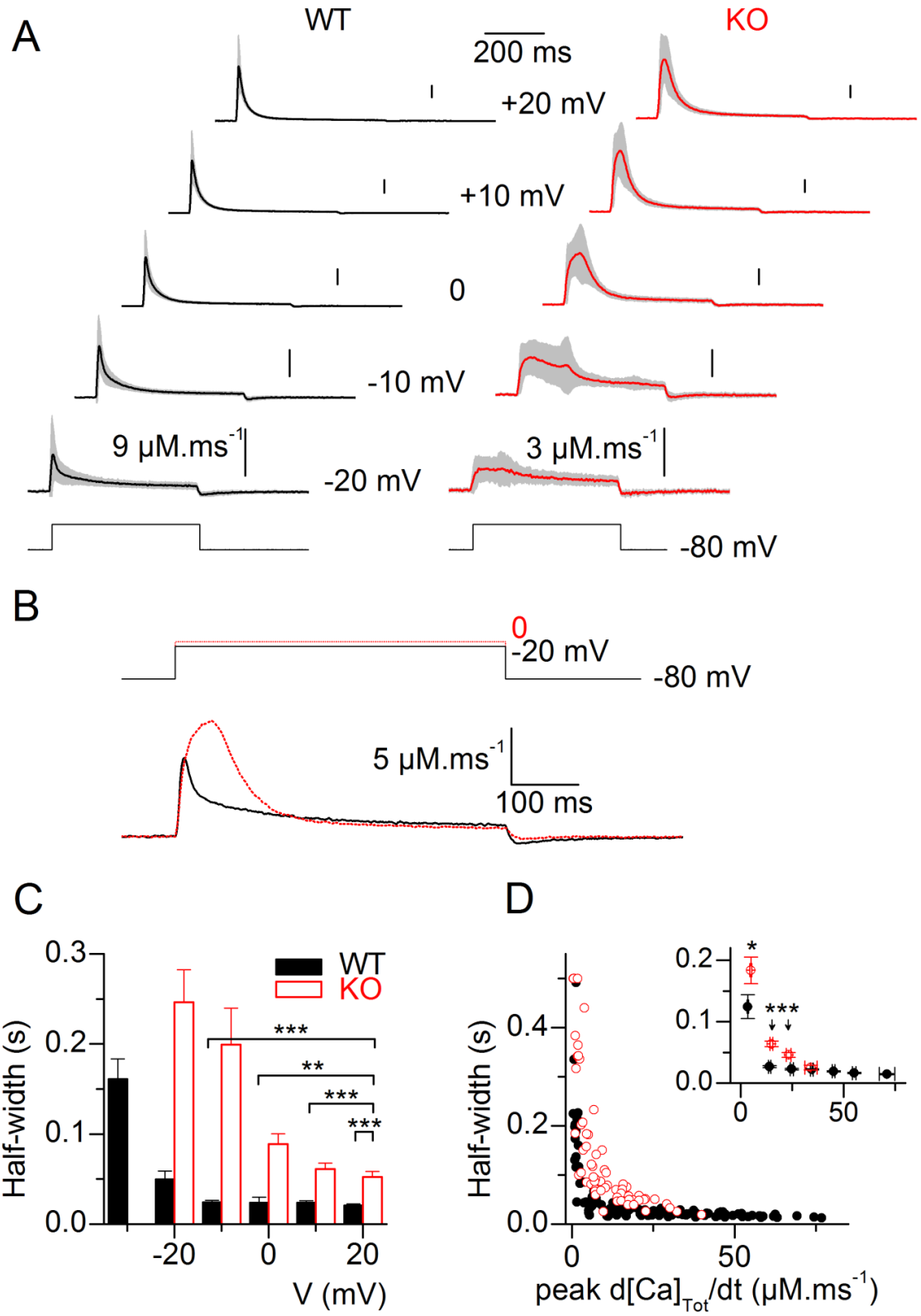
A
WT
KO
200 ms
+20 mV
+10 mV
0
-10 mV
9 µM.ms-1
-20 mV
3 µM.ms-1
-80 mV
B
0
-20 mV
-80 mV
5 µM.ms-1
100 ms
C
WT
KO
Half-width (s)
0.3
0.2
0.1
0.0
***
**
***
***
-20
0
20
V (mV)
D
Half-width (s)
0.4
0.2
0.0
0.2
0.1
0.0
*
***
0
50
0
50
peak d[Ca]Tot/dt (µM.ms-1)

Fig.3

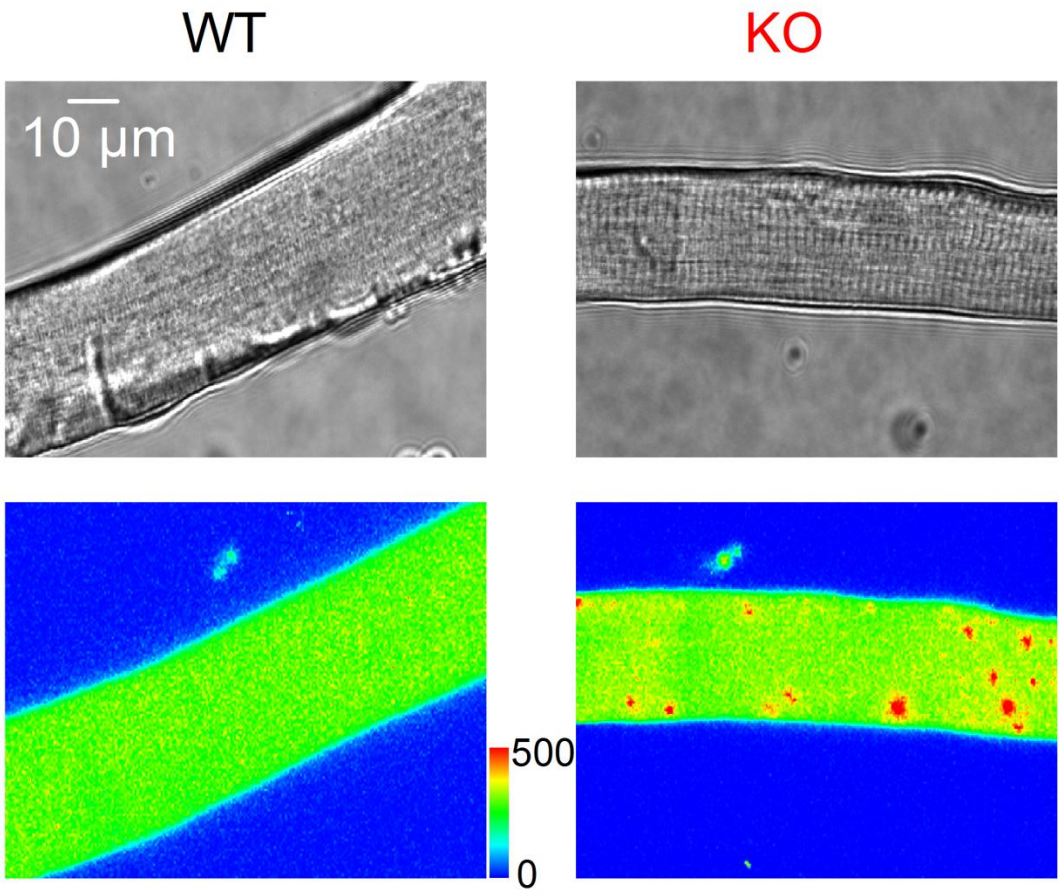

Fig. 4

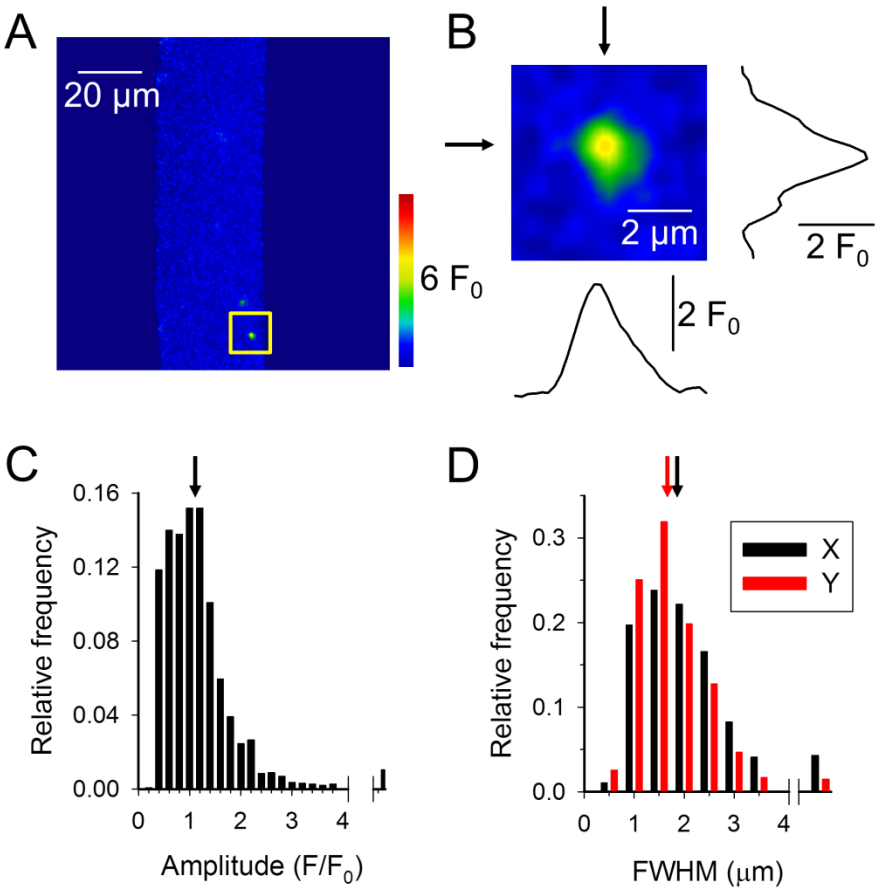
A
20 μm
6 F0
B
2 μm
2 F0
2 F0
C
Relative frequency
0.16
0.12
0.08
0.04
0.00
0 1 2 3 4
Amplitude (F/F0)
D
Relative frequency
0.3
0.2
0.1
0.0
X
Y
0 1 2 3 4
FWHM (μm)

Fig.5

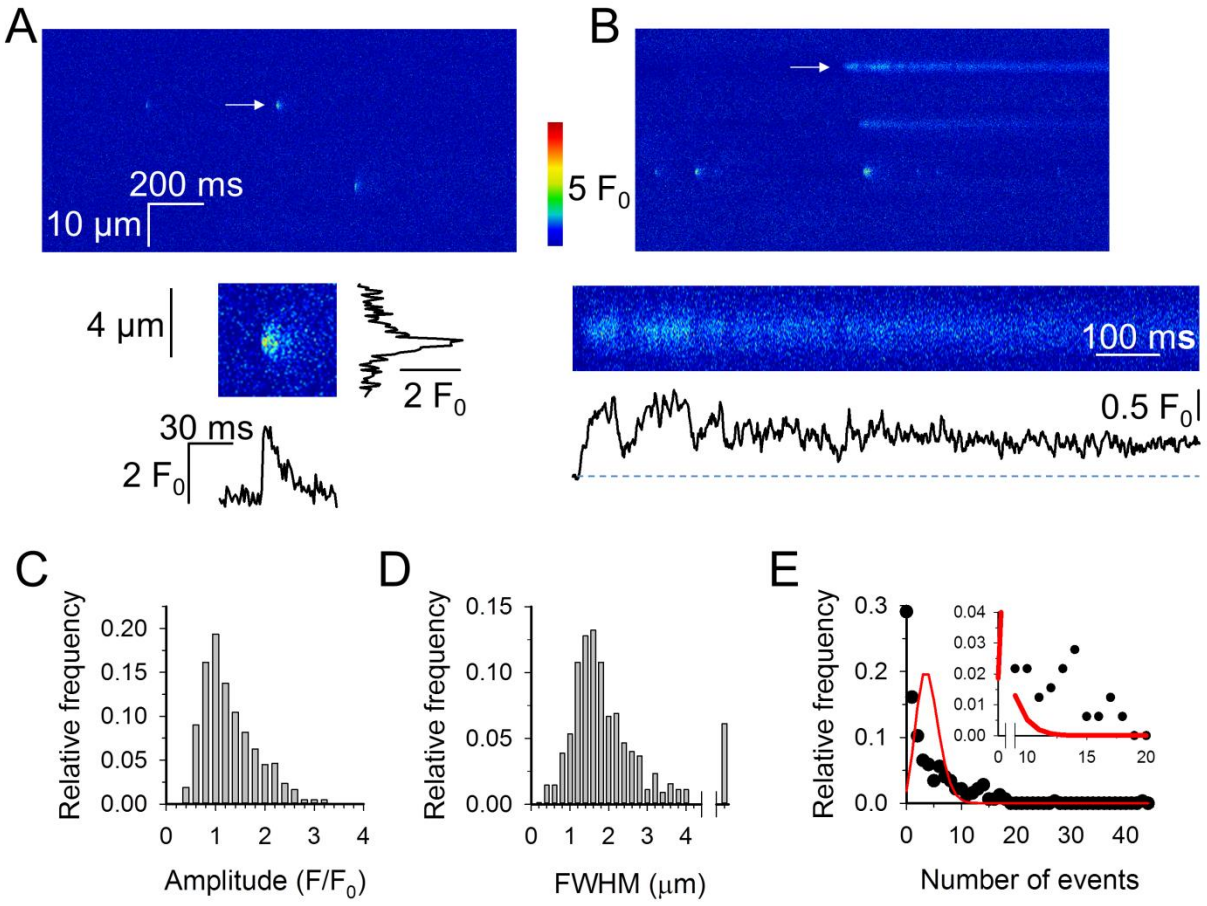
A
B
200 ms
10 μm
5 F0
4 μm
2 F0
30 ms
2 F0
100 ms
0.5 F0
C
Relative frequency
Amplitude (F/F0)
D
Relative frequency
FWHM (μm)
E
Relative frequency
Number of events

Fig.6

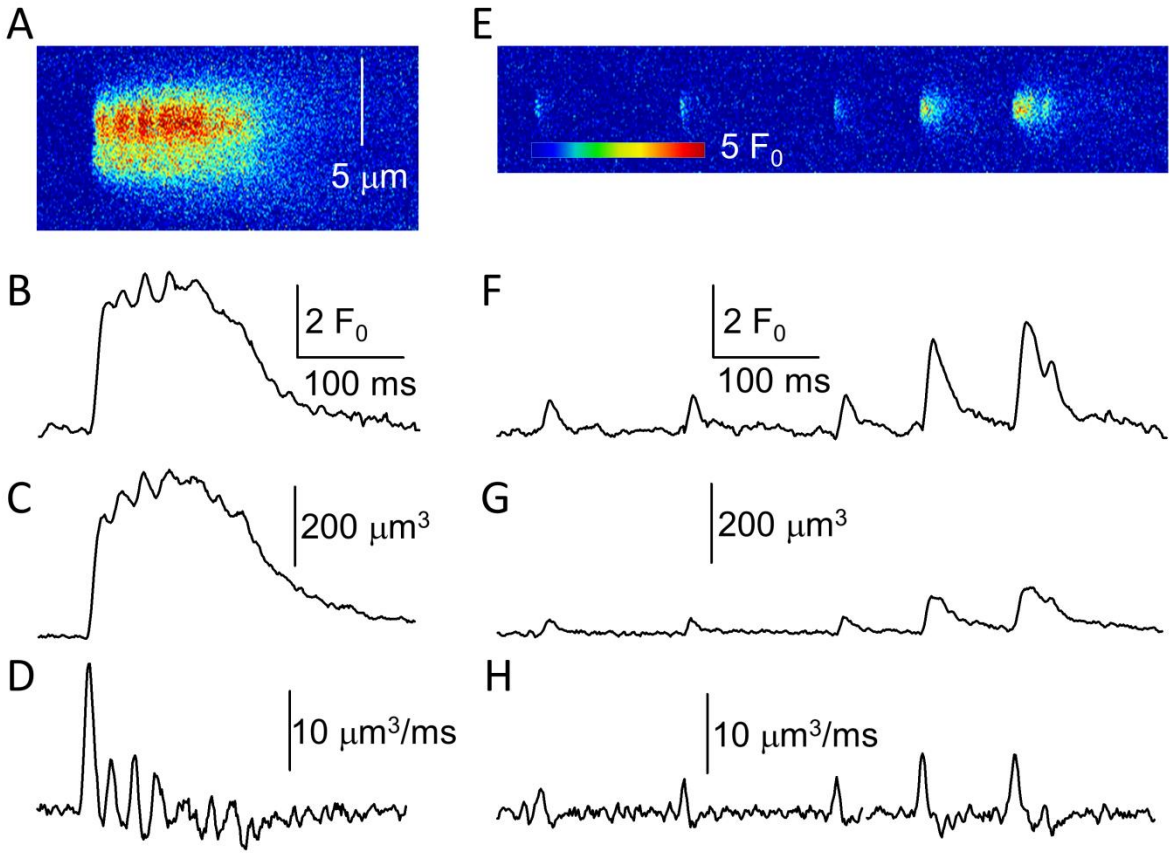
A
5 μm
E
5 F0
B
2 F0
100 ms
F
2 F0
100 ms
C
200 μm3
G
200 μm3
D
10 μm3/ms
H
10 μm3/ms

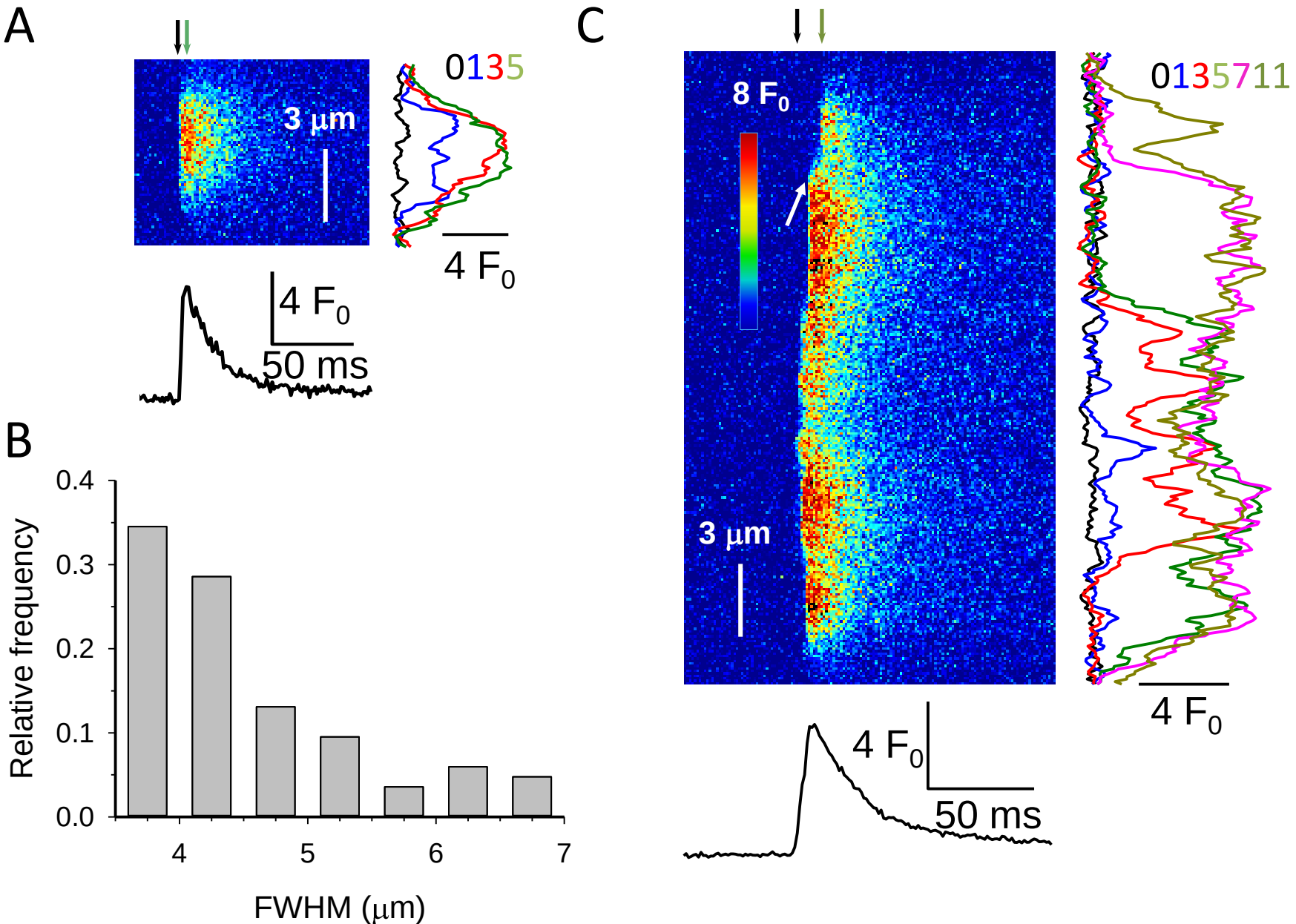
A
3 µm
0135
4 F0
4 F0
50 ms
B
Relative frequency
0.4
0.3
0.2
0.1
0.0
4
5
6
7
FWHM (µm)
C
8 F0
3 µm
0135711
4 F0
4 F0
50 ms

Fig. 8

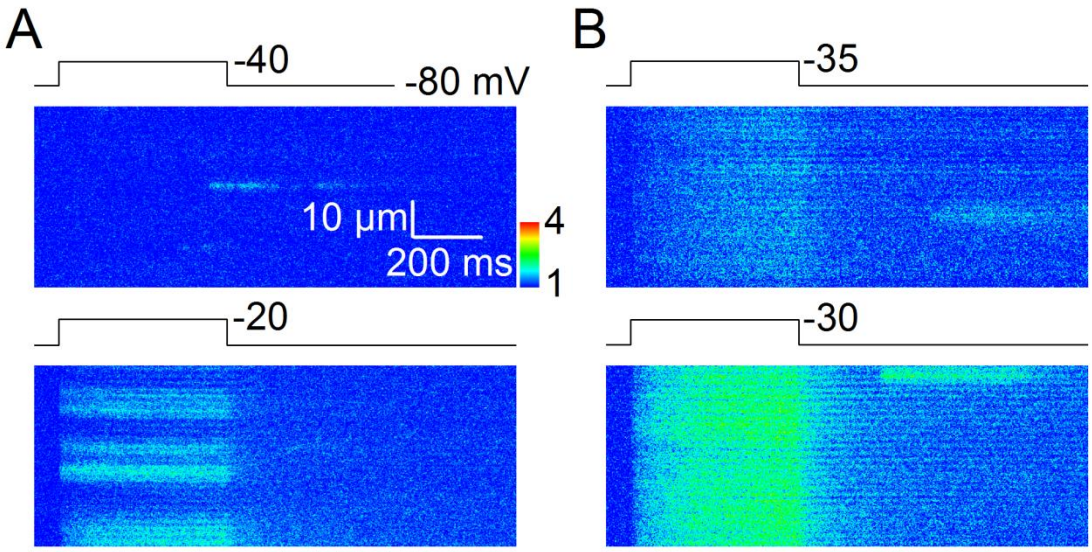

Healthy RyR1-mediated
SR Ca^{2+} release

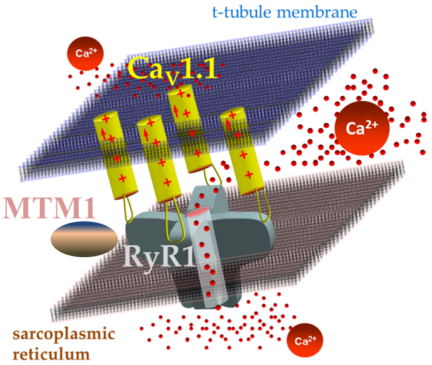

Ca^{2+}-induced Ca^{2+} release
in myotubular myopathy